

# Spectral analysis of the free surface fluctuations behind microbreakers

Alessandro Iafrati and Emilio F. Campana, INSEAN (Italian Ship Model Basin),  
E-mail: a.iafrati@insean.it, e.campana@insean.it

## 1. INTRODUCTION

Small-scale surface fluctuations taking place behind steady breaking waves has received attention in quite distinct research frameworks, from naval hydrodynamics to geophysical applications, with many papers primarily concerned with the remote sensing, radar or infrared, of the ocean surface (see [1] and [11], for instance). Short-wavelength spilling breakers, also referred as ‘microbreakers’ are usually originated by the wind and play an important role in terms of momentum, heat and gas exchange between atmosphere and ocean. At this short scales, due to the strong action of surface tension, the characteristic plunging jet is replaced by a bulge which slides down along the forward face of the wave [12]. Since the breaking takes place without wave overturning, the amount of air entrained is significantly reduced [8].

The generation and the downstream propagation of free surface ripples have been subject of intense research studies. In [6], by using the dispersive focusing technique, very gentle breakers have been generated experimentally by progressively reducing the amplitude of the wavemaker motion. It has been shown that, at the early stage of the breaking establishment, the bulge grows while the toe is substantially fixed with respect to the crest. In a next stage, the bulge begins to slide down upon the forward face of the wave and a shear layer develops between the gravity induced downslope flow near the free surface and the underlying upslope flow. Instabilities of this shear layer eventually lead to the formation of a train of downstream propagating ripples. In [7] and [5] a submerged hydrofoil has been used to produce a quasi-steady breaking and the frequency and wavenumber spectra of the downstream propagating surface fluctuations have been analysed. Comparisons with a theoretical model confirmed that shear flow instabilities are the primary mechanism for ripples generation.

An accurate analysis of the space-time behaviour of the surface fluctuations behind steady breakers has been carried out also in [13]. Wavenumber-frequency spectra show that ripples’ wavelength grows during their downstream motion while the temporal frequency of fluctuations, recorded at different longitudinal position, remains substantially constant. This led authors to speculate that ripples behaves like surface waves on a spatially varying current.

## 2. NUMERICAL MODEL

In this paper small scale breakers generated by a submerged hydrofoil are numerically studied by solving the two-dimensional unsteady Navier–Stokes equations for the two-phase flow of air and water. A significant reduction of the computational effort is achieved by using the heterogeneous domain decomposition approach developed in [3]. With this approach a potential flow approximation is used in a subdomain about the hydrofoil and a suitable matching condition has been developed to exchange information between the viscous flow region about the interface and the potential flow region about the hydrofoil.

The two-fluid Navier–Stokes solver is coupled with a Level-Set technique for the interface capturing thus allowing the description of free surface motion even in the presence of complex interface topologies. The jump in the physical properties of the two fluids is spread across a small region about the interface. Surface tension effects are modeled as a continuum force by using the model originally proposed in [2]. A more detailed discussion of the coupling strategy and of the numerical method can be found in [10].

## 3. THE GENERATION OF FREE SURFACE RIPPLES

By using the model discussed above, the unsteady free surface flow generated by a submerged hydrofoil starting from rest has been numerically simulated. Some scale effects on the wave breaking establishment and the formation of downstream propagating surface ripples have been discussed in [4] and in [9]. In the latter, a careful analysis of the flow field taking place beneath the free surface has been carried out aimed at investigating the mechanisms governing formation and downstream propagation of the surface ripples.

In figure 1 some results are shown in terms of vorticity fields for the simulation at  $Re = 2537$ ,  $Fr = 0.567$ ,  $We = 10.55$ . Results show the sequence of vorticity fields ranging from the initial downslope motion of the bulge until the beginning of the ripples generation. The instantaneous vorticity fields clearly display the initial growth of the shear flow instabilities developing between the fluid inside the bulge, which is moving upstream, and the incoming upslope flow.

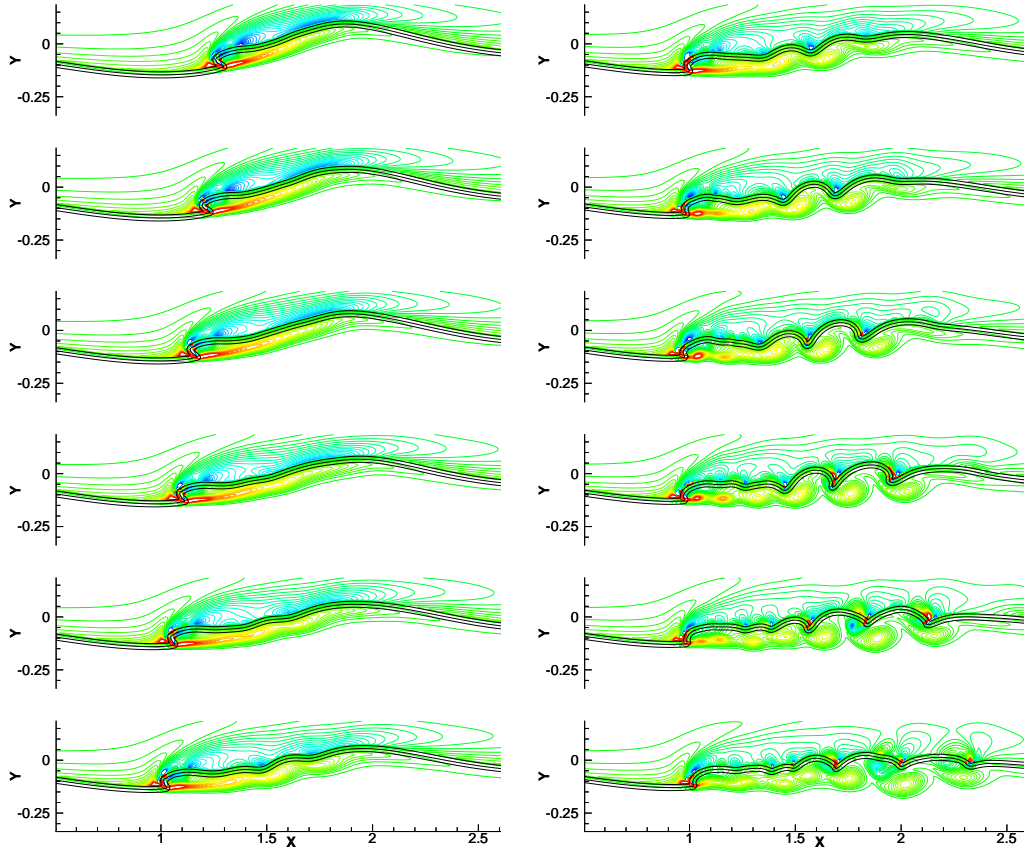


Figure 1: Sequence showing free surface profiles and vorticity contours during the first downslope motion of the bulge, as seen in the hydrofoil frame of reference ( $We = 10.55$ ,  $Fr = 0.567$ ,  $Re = 2537$ ). The three black lines represent density contours at three different density values:  $\rho/\rho_w = 0.03, 0.5, 1$ . Configurations refer to the interval  $t = 14$  to  $t = 16.2$  with a time interval among successive configurations  $\Delta t = 0.2$ . The development of shear flow instabilities and the corresponding formation of free surface ripples is clearly shown. Secondary vorticity also appears as a result of the interaction of primary coherent structures with the highly curved troughs.

At a later stage, instabilities lead to the formation of separated coherent structures that strongly interact with the free surface, giving rise to ripples on the free surface which are tracks of the vortex structures lying beneath. The interaction of the vortex structure with the free surface is responsible for the formation of a scar, which corresponds to the ripple trough, just downstream the vortex structure itself. In the early stage after their appearance, ripples grow in amplitude while the wavelength is essentially related to the distance between two adjacent coherent structures. Hence, the ripples wavelength grows during the downstream motion of the vortex structures, due to both the growing distance between adjacent structures and the diffusion process of the single structure.

At a later stage, the intense interaction between vorticity and the highly curved free surface is responsible for the production of secondary vorticity shed into the

water, as it clearly highlighted by the last three configurations in figure 1. The maximum intensity of the secondary vorticity can be even large than that of the corresponding primary structures. The velocity field developing after secondary structures appear, acts to hold back the primary ones, thus leading to the formation of vortex pairs. Due to the self-induced velocity field, vortex pairs are “overtaken” by the associated troughs which, therefore, experience a reduction of their curvature.

#### 4. SPACE-TIME ANALYSIS OF FREE SURFACE FLUCTUATIONS

With the aim of evaluating the main features of their downstream propagation, spectral analysis in space and time are performed on the basis of the instantaneous measurements of the free surface elevation immediately

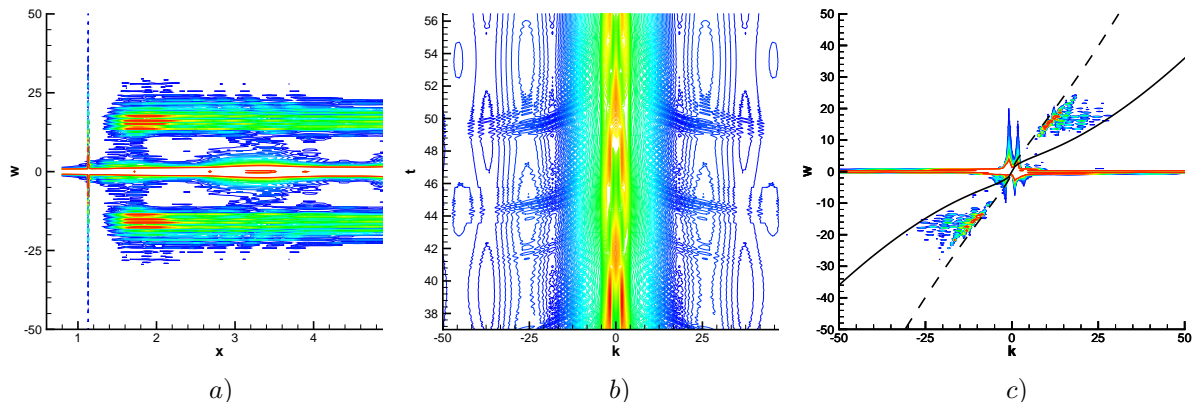


Figure 2: Frequency and wave-number spectra of the free surface fluctuations. On (a), the frequency spectrum is plotted at different longitudinal positions in the frame of reference attached to the hydrofoil. On (b) the wavenumber spectrum is plotted at different time and on (c) the  $k - \omega$  spectra is drawn.

ahead and behind the breaking region. By following what done in [13] and [5], frequency and wave-number spectra are calculated and plotted versus longitudinal position and time, respectively. In order to evaluate the spectra, the free surface elevation obtained for the numerical simulation is sampled with  $\Delta t = 0.005$  in the interval  $t = 37$  to  $t = 56$  and, in space, with  $\Delta x = 0.01$  in the range  $x = 0.8$  to  $x = 4$ . The horizontal extension of this window is chosen as large as one and half wavelengths (based on the linear theory). The frequency-wave-number spectrum is evaluated as

$$S(k, \omega) = \iint \eta(x, t) e^{i(\omega t - kx)} d\omega dk .$$

In figure 2a the contours of the frequency components of the free surface fluctuations are shown versus the streamwise location. As discussed in [13], this graph clearly displays the existence of two distinct components: (i) a low frequency one, related to the surge motion of the toe and (ii) a higher frequency component, due to the downstream propagation of the ripples. From these results, it can be seen that the high frequency component, centered about  $|\omega| = 15$ , is related to the downstream propagation of the ripples. The vertical contour levels about  $x = 1.15$  represent the broadband frequency components associated with the motion of the sharp front of the bulge.

The high frequency component is ascribed to the ripples propagation since this contribution only appears downstream the position of the top of the bulge. The frequency components associated to the ripples formation and propagation exhibit a rapid initial growth from  $x \sim 1.4$  to  $x \sim 1.8$ . Further downstream, but for a weak reduction in the amplitude taking place up to  $x \sim 2.2$ , they remain nearly constant. These results are in a

qualitative good agreement with what found by [13], and the larger decay rate observed in the experiments can be attributed to the differences in the flow conditions and to the two-dimensional assumption made in the present numerical computations.

With regards to the spatial Fourier transform, in figure 2b the wavenumber spectrum is displayed versus time. This picture clearly show that, periodically, components at short wavelength appear about  $|k_x| = 25$ . As the time elapses, that is during the downstream propagation, the ripples' wavelength grows. This aspect agrees with what discussed in [13].

On the basis of the above considerations, it follows that the ripples wavelength grows during their downstream motion while no substantial changes occur in terms of frequency components. This fact led [13] to speculate that the behavior is “consistent with the idea of waves propagating on a spatially varying current”. In order to further support this idea, in [13] the dispersion relation given by linear theory

$$\omega = (gk_x + \sigma k_x^3)^{1/2} + Uk_x, \quad (1)$$

is plotted on the wavenumber-frequency spectra by using  $U = 0$  and  $U = U_r$ . In figure 2c the same graph is drawn on the basis of the present numerical results. As already stated, the oscillating motion of the toe is associated with small frequencies while high frequency components at short wavelength are instead induced by the sharpness of the bulge front. Downstream propagating free surface ripples manifest themselves at higher wavenumbers with  $\omega$  ranging from  $10 \rightarrow 30$ .

As discussed in [13], ripples are generated in the breaking region where the fluid is almost at rest in the hydrofoil frame of reference and the dispersion relation with  $U = 0$  (solid line in figure 2c) provides a higher

bound for the ripples wavenumber. As they propagate downstream, thus reducing their wavenumber components, the underlying current is accelerating and then the dispersion relation with  $U = U_r$  is progressively approached (dash line in figure 2c).

In order to get a better understanding of the free surface fluctuations, its power spectrum  $S$  is evaluated as

$$S(\omega) = \frac{|X_T(\omega)|^2}{T}$$

and plotted on figure 3 for the half plane  $\omega > 0$  only. On the same graph, the power law  $\omega^{-7/2}$  found in [7] on the basis of their experimental measurements is also plotted. From this graph it can be seen that the power spectrum of the numerical results follows the power law  $\omega^{-15/2}$  which is significantly different from the experimental value. We believe that this different behaviour has to be ascribed to the lack of three-dimensional effects on our numerical simulation. This hypothesis is supported by the fact that in [7] some two-dimensional results obtained by using an Euler solver to study the evolution of periodic shear flow beneath the free surface are shown which appear to follow a  $\omega^{-10}$  power law. The difference between our numerical results and those discussed in [7] is likely due to the differences in the governing equations and in the boundary conditions.

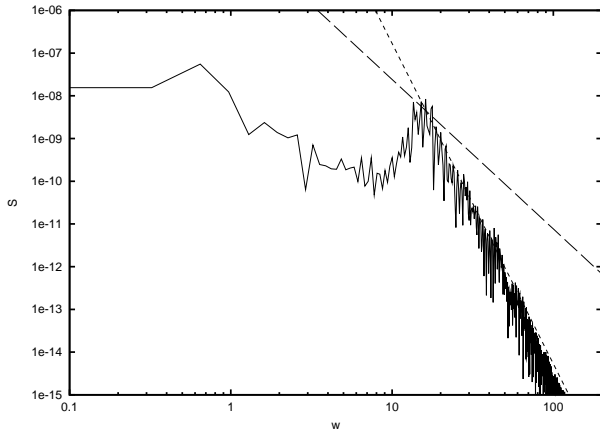


Figure 3: Power spectrum of the free surface fluctuations at  $x = 1.75$ . The dashed line represents the  $\omega^{-7/2}$  power law found in [7] (on the basis of the experimental measurements) while the dotted line represents the  $\omega^{-15/2}$  power law.

## 1 Acknowledgments

This work was partially supported by the *Office of Naval Research*, under grant N.000140010344, through Dr. Pat Purtell.

## References

- [1] BANNER, M.L. & FOOKS, E.H. 1985 On the microwave reflectivity of small-scale breaking water waves. *Proc. R. Soc. Lond. A* **399**, 93–109.
- [2] BRACKBILL, J.U., KOTHE, D.B., & ZEMACH, C. 1992 A continuum method for modeling surface tension. *J. Comput. Phys.* **100**, 335–354.
- [3] CAMPANA, E.F. & IAFRATI, A. 2001 Unsteady free surface waves by domain decomposition approach. *Proc. 16th IWWF - Hiroshima (Japan)*, 9–13.
- [4] CAMPANA, E.F. & IAFRATI, A. 2002 Surface tension effects on breaking waves. *Proc. 17th IWWF - Cambridge (UK)*, 21–24.
- [5] COAKLEY, D.B. & DUNCAN, J.H. 1996 The flow fields in steady breaking waves. *Proc. 21st Symp. on Naval Hydrodynamics*, pp. 534–549.
- [6] DUNCAN, J.H., PHILOMIN, V., BEHRES, M. & KIMMEL J. 1994 The formation of spilling breaking water waves. *Phys. Fluids* **6**, 2558–2560.
- [7] DUNCAN, J.H. & DIMAS, A.A. 1996 Surface ripples due to steady breaking waves. *J. Fluid Mech.* **329**, 309–339.
- [8] DUNCAN, J.H. 2001 Spilling Breakers. *Annu. Rev. Fluid Mech.* **33**, 519–547.
- [9] IAFRATI, A. & CAMPANA, E.F. 2002 Direct numerical simulation of surface tension dominated and non-dominated breaking waves. *Proc. 24th ONR Symp. on Naval Ship Hydrodynamics - Fukuoka (Japan)*, (on CDrom).
- [10] IAFRATI, A. & CAMPANA, E. F. 2003 A domain decomposition approach to compute wave breaking. *Int. J. Numer. Meth. Fluids* **41**, 419–445.
- [11] SIDDIQUI, M.H.K., LOEWEN, M.R., RICHARDSON, C., ASHER, W.E. & JESSUP, A.T. 2001 Simultaneous particle image velocimetry and infrared imagery of microscale breaking waves. *Phys. Fluids* **13**, 1891–1903.
- [12] TULIN, M.P. 1996 Breaking of ocean waves and downshifting. *Waves and Nonlinear Processes in Hydrodynamics* (eds. J. Grue B. Gjevik & J.E. Weber), pp. 170–190. Kluwer.
- [13] WALKER, D.T., LYZENGA, D.R., ERICSON E.A. AND LUND, D.E. 1996 Radar backscatter and surface roughness measurements for stationary breaking waves. *Proc. Roy. Soc. London A* **452**, 1953–1984